HHS Public Access

Author manuscript

Stem Cells. Author manuscript; available in PMC 2016 August 01.

Published in final edited form as:

Stem Cells. 2015 August ; 33(8): 2483–2495. doi:10.1002/stem.2052.

IGF1 Promotes Adipogenesis by a Lineage Bias of Endogenous Adipose Stem/Progenitor Cells

Li Hu[1,2,#], **Guodong Yang**[2,#], **Daniel Hägg**[2,#], **Guoming Sun**[2], **Jeffrey M. Ahn**[3], **Nan Jiang**[2], **Christopher L. Ricupero**[2], **June Wu**[4], **Christine Hsu Rodhe**[4], **Jeffrey A. Ascherman**[4], **Lili Chen**[1,*], and **Jeremy J. Mao**[2,*]

[1]Department of Stomatology, Union Hospital, Tongji Medical College, Huazhong University of Science and Technology, 1277 JieFang Avenue, Wuhan, Hubei 430022, P.R. China

[2]Center for Craniofacial Regeneration (CCR), Columbia University Medical Center, 630 W. 168 St. – PH7E, New York, NY 10032, USA

[3]Department of Otolaryngology, Columbia University Medical Center 630 W. 168St, New York, NY10032, USA

[4]Department of Plastic Surgery, Columbia University Medical Center 630 W. 168St, New York, NY10032, USA

Abstract

Adipogenesis is essential for soft tissue reconstruction following trauma or tumor resection. We demonstrate that CD31-/34+/146− cells, a subpopulation of the stromal vascular fraction (SVF) of human adipose tissue, were robustly adipogenic. Insulin Growth Factor-1 (IGF1) promoted a lineage bias towards CD31-/34+/146− cells at the expense of CD31-/34+/146+ cells. IGF1 was microencapsulated in poly(lactic-co-glycolic acid) scaffolds and implanted in the inguinal fat pad of C57Bl6 mice. Control-released IGF1 induced remarkable adipogenesis *in vivo* by recruiting endogenous cells. In comparison with the CD31-/34+/146+ cells, CD31-/34+/146− cells had a weaker Wnt/β-catenin signal. IGF1 attenuated Wnt/β-catenin signaling by activating Axin2/PPARγ pathways in SVF cells, suggesting IGF1 promotes CD31-/34+/146− bias through tuning Wnt signal. PPARγ response element (PPRE) in Axin2 promoter was crucial for Axin2 upregulation, suggesting that PPARγ transcriptionally activates Axin2. Together, these findings illustrate an Axin2/PPARγ axis in adipogenesis that is particularly attributable to a lineage bias towards CD31-/34+/146− cells, with implications in adipose regeneration.

[*]Co-corresponding authors: Jeremy J. Mao, Professor and Edwin S. Robinson Endowed Chair, Columbia University Medical Center, 630 W. 168 St. – PH7E - CDM, New York, NY 10032, Phone: 212-305-4475, Fax: 212-342-0199, jmao@columbia.edu. Lili Chen, Professor, Department of Stomatology, Union Hospital, Tongji Medical College, Huazhong University of Science and Technology, 1277 JieFang Avenue, Wuhan, Hubei 430022, P.R.China, Tel: 86-27-85726949;, chenlili@whuh.com.
[#]Co-first authors

Author Contribution

L.H. was responsible for primary technical undertaking including most *in vitro* experiments, collected and analyzed data and drafted the manuscript. G.Y. contributed to experimental design and performed several *in vitro* signaling experiments. D.H. performed *in vivo* experiments and collected data. G.S. contributed to analysis of IGF1 controlled release data. N.J. assisted to debug several *in vitro* experiments. J.M.A., C.H.R. and J.A.A. provided clinical samples and translational aspects of soft tissue reconstruction. L.C. co-mentored L.H. and provided financial sponsorship. J.J.M. conceived and designed the experiments, and oversaw the collection of results, data interpretation and finalized the manuscript.

Keywords

adipose; mesenchymal; stem cells; SVF; IGF1; PPARγ; Axin2; CD146

Introduction

Adipogenesis has recently received robust attention due to its relevance to obesity, diabetes and clinical needs for innovative surgical reconstruction of soft tissue defects following tumor resection, infections or trauma [1–4]. The stromal vascular fraction (SVF) of the white adipose tissue harbors stem/progenitor cells [5–9]. When isolated as mononuclear and adherent cells, similar to bone marrow mesenchymal stem/stromal cells, SVF cells undergo limited expansion *ex vivo* and are capable of differentiating into adipocytes [10], thus named as adipose stem cells (ASCs). However, SVFs or ASCs are highly heterogeneous [11–13]. For example, CD31-/34+ fractions of SVF cells have robust capacity to differentiate into adipocytes [14], relative to their parent populations [15]. Similarly, Lin/CD29+/CD34+/Sca-1+/CD24+ cells isolated from adult white adipose tissue are also highly adipogenic [16, 17], and derive from platelet-derived growth factor receptor α labeled stem/progenitor cells. Obesity, which is typically systemic adipogenic gain, is in sharp dichotomy to a strong clinical need for focal reconstruction of soft tissue. Molecular signaling mechanisms of adipogenesis are only fragmentally understood, and may present common threads between systemic and focal adipogenic gain.

The processes by which adipose stem/progenitor cells differentiate into mature adipocytes are governed by an incompletely understood array of transcriptional factors, cell-cycle regulators, and other co-factors [18–20]. Sequential induction of Krox20 (Egr2) [21], Klf4 [22, 23], C/EBPδ, C/EBPβ, C/EBPα [24–26], TRAP220 and PPARγ [27–29] has been connected to multiple adipogenesis steps. Among these transcription factors, PPARγ is a member of the nuclear receptor superfamily and among few presently known gatekeepers of adipogenesis [30, 31]. Wnts (Wingless-type MMTV integration site family members) are secreted glycoproteins that regulate tissue homeostasis and remodeling [32–34]. Both canonical Wnt (including β-catenin) and non-canonical Wnt pathways have been recently shown to regulate adipogenesis [35–38]. Increased activation of β-catenin resulted in decreased expression of PPARγ target genes in 3T3-L1 cells [39]. Reciprocally, PPARγ activation suppresses Wnt/β-catenin signaling in adipogenesis [40–42]. However, little is known of a potential crosstalk between Wnt and PPARγ in subpopulations of adipose stem/progenitor cells.

Experimental effort for novel soft tissue reconstruction has relied on the transplantation of stem/progenitor cells that are typically isolated from adipose tissue. However, the downside of cell transplantation in adipose regeneration is costs and potential complications associated with *ex vivo* cell cultivation [43]. Is it possible to learn and apply molecular promoters of adipogenesis towards soft tissue reconstruction by a cell-free approach? Here, we first discovered that CD31-/34+/146− cells, a subpopulation of SVF cells of lipectomized human adipose tissue, were robustly adipogenic than their parent SVF cells. Insulin Growth Factor-1 (IGF1) not only promoted a lineage bias towards CD31-/34+/146− cells, but also

promoted *in vivo* adipogenesis, when delivered by controlled release in the inguinal fat pad of C57Bl6 mice, without cell transplantation. *De novo* adipose tissue was formed within poly(lactic-co-glycolic acid) scaffolds by IGF1 recruited cells, predominantly CD31-/34+/146− cells that were derived entirely from the host. IGF1 activated Axin2/PPARγ pathways in SVF and CD31-/34+ cells, regardless of CD146 polarity. IGF1 induces adipogenesis by exerting multifaceted roles: inducing a lineage bias towards CD31-/34+/146− cells, upregulating Axin2/PPARγ and reducing the intrinsic Wnt/β-catenin set. Collectively, these findings provide important clues for manipulating IGF1, PPARγ and Axin2 for opposite goals of attenuating obesity or promoting focal adipose regeneration.

Results

CD31-/34+/146− cells had robust adipogenic capacity

Adipose stem/progenitor cells (ASCs) are typically identified as mononucleated adherent cells isolated from adipocyte tissue [44]. We first asked whether robustly adipogenic fractions of isolated ASCs, such as CD31-/34+ cells [45], all originate from the vascular wall, given the innate location of blood vessel bundles among clusters of adipocytes. Immunofluorescent staining of the surgically removed human abdominal subcutaneous adipose tissue showed that about 20%–50% of the CD34 (mesoderm stem cell marker) positive cells were also CD146 positive, a hallmark of pericytes [46–48] (Fig. 1A–D; Supplementary Fig. 2A–D). In addition, some of the CD146+ cells were CD31 (PECAM) positive, while others were just adjacent to CD31 cells (Fig. 1E–H; Supplementary Fig. 2E–H). All of these data suggest that there might be two populations of adipogenic stem cells in the adipose tissue: CD31-/34+/146− and CD31-/34+/146+. To further confirm the detailed percentages of CD31-/34+/146− and CD31-/34+/146+, adipogenic stem cells were isolated and subjected to flow cytometry analysis. Flow cytometry analysis showed that 94.5±3.6% of stromal vascular fraction (SVF) cells at passage 1 (p1) were CD31-/34+ cells, which are known to be robustly adipogenic[45]. Among passage 1 (p1) CD31-/34+ cells, 20.7±1.7% were CD146 negative, whereas 59.5±2.8% were CD146+ cells (Fig. 1I). Notably, the percentage seemed not perfectly correlated with the immunostaining data, which might be due to the sensitivity differences between the two assays. Alternatively, the cell culture procedure changed the percentage. By p3, CD31-/34+/146− cells decreased to 11.2±1.0% (Fig. 1J), whereas CD31-/34+/146+ cells increased to 71.2±1.6% (Fig. 1J). The decrease of CD34 and CD146 in our experiment was consistent with previous studies [49, 50].

Next we explored whether CD146 positivity among CD31-/34+ cell fractions made a difference in adipogenesis. SVF cells (p1) differentiated into adipocytes (Fig. 1K), in consistency with previous work by us and others [51]. CD31-/34− cells, however, showed relatively modest adipogenesis capacity (Fig. 1L), similar to CD31-/34+/146+ cells (Fig. 1M). Remarkably, CD31-/34+/146− cells demonstrated nearly 2 fold higher adipogenic capacity (Fig. 1N, Supplementary Fig. 3). Furthermore, expression of PPARγ and FABP4 expression in CD31-/34+/146− cells were 2 and 5 fold of that in CD31-/34+/146+ cells (Fig. 1O), which were also significantly higher than that in SVF and CD31-/CD34− cells. In contrast, about 70% of CD31-/34+/146+ cells were Ki67 positive, while only 35% of

CD31-/34+/146− cells were Ki67 positive (Fig. 1P–1R). Cell proliferation assay by CCK-8 further confirmed CD31-/34+/146+ cells had stronger proliferation capability (Fig. 3F).

For osteogenesis, SVF cells showed remarkable ability to differentiate along the osteogenic lineage in chemically defined medium (Fig. 1S). CD31-/34− cells, however, were hardly osteogenic when exposed to the same osteogenesis induction medium (Fig. 1T). Strikingly, CD31-/34+/146+ cells showed robust ability to differentiate into osteoblast-like cells (Fig. 1U). In contrast, CD31-/34+/146− cells showed diminished ability to differentiate into osteoblast-like cells (Fig. 1V). Thus, CD146 negativity perhaps defines a subpopulation of adipogenic stem/progenitor cells (ASCs or SVFs) that are not perivascular, slowly proliferative and yet robustly adipogenic. Together, these findings suggest that CD146 polarity among CD31-/34+ cells defines adipogenic progenitors (CD31-/34+/146− cells).

Wnt/β-catenin and PPARγ interplay in CD31-/34+ cells

Given that Wnt/β-catenin signaling attenuates adipogenesis of ASCs or SVF cells [52], we exploited the interplay between Wnt/β-catenin and PPARγ signaling in CD31-/34+/146+/− cells that showed robust differences in adipogenesis (Fig. 1M, N). The intensity and nuclear β-catenin staining in CD31-/34+/146+ cells was significantly higher than that in CD31-/34+/146− cells (Fig. 2A–G). Consistently, CD31-/34+/146+ cells showed significant higher nuclear β-catenin expression, as revealed by Western blot, in comparison to CD31-/34+/146− cells (Fig. 2H). We then transfected a TOPflash reporter separately into CD31-/34+/146+ and CD31-/34+/146− cells, and found that CD31-/34+/146+ cells had significantly stronger Wnt luciferase activity and significantly greater cyclin D1 expression than CD31-/34+/146− cells (Fig. 2I), further suggesting higher innate Wnt activity and proliferation capacity in CD31-/34+/146+ cells, but nonetheless a modest innate Wnt set level in CD31-/34+/146− cells that are robustly adipogenic.

PPARγ expression in CD31-/34+ cells was virtually unresponsive to Wnt3a protein (10 ng/mL) in growth medium, regardless of CD146 polarity (Fig. 2J), suggesting that CD31-/34+ cells are not spontaneously adipogenic, with or without Wnt3a interference. PPARγ expression was significantly reduced to 30% upon exposure to Wnt3a protein in chemically defined adipogenesis induction medium in CD31-/34+/146− cells (Fig. 2J). Similar trends were observed in CD31-/34+/146+ cells, despite a significantly lower fold change (Fig. 2J). Conversely, overexpression of PPARγ in both CD31-/34+/146+ and CD31-/34+/146− cells attenuated Wnt (TOPflash luciferase) activity in either growth medium or adipogenesis induction medium, with significantly higher basal Wnt activity and greater fold change in CD31-/34+/146+ cells (Fig. 2K). All of these suggest that PPARγ and Wnt are mutually inhibitive and the differences in PPARγ and Wnt activity should be the characteristics of CD31-/34+/146+/− cells.

IGF1 promoted a lineage bias towards CD31-/34+/146− cells

IGF1 plays important roles in regulating the fate of adipocytes [53]. However, whether IGF1 contributes to adipogenesis by promoting a fractional bias among adipose stem/progenitor cells is unknown. Accordingly, we tested the hypothesis that IGF1 stimulates a lineage bias among SVF cells and/or CD31-/34+ cells. First, we were surprised that IGF1 induced little

change in the percentage of CD31-/34+ cells (Fig. 3A, B). Strikingly though, IGF1 treated SVF cells had a significant increase in CD146− cells among the native CD31-/34+ fraction (Fig. 3A, B), and a concomitant decrease in CD146+ cells (Fig. 3A, B). To further confirm the role of IGF1 on the bias towards CD31-/34+/146−, we sorted CD31-/CD34+/146+ cells and treated with IGF1. Treatment of IGF1 on CD31-/CD34+/146+ cells didn't change the percentage of CD31-/34+, although they decreased to 25% upon culture, which was consistent with the gradual loss of CD34 upon culture (Fig 1J). However, IGF1 also promoted CD146− cell percentage in the CD31-/34+ population (Fig 3C, D). When tabulated, IGF1 application had little effect on CD31-/34+ cell fractions among SVFs (Fig. 3E, left 2 columns), but significantly increased CD146− cell fractions (from 11.8±1.2% to 20.2±1.5%) at the cost of CD146+ cells (from 70.7±1.4% to 58.1±3.0%), suggesting an IGF1 induced a lineage bias towards CD31-/34+/146− cells that are robustly adipogenic, as we showed above. To exclude the possibility that IGF1 promoted cell bias is due the proliferation bias, proliferation rate of IGF1 stimulated cells were tested. The proliferation of CD31-/34+ cells, regardless of CD146 polarity, responded similarly to IGF1 (Fig. 3F).

Furthermore, IGF1 stimulated the proliferation of SVF cells in a dose dependent manner (Fig. 4A) and independently induced adipogenesis with or without insulin (Fig. 4B, C). We also tested whether IGF1 was chemotactic for adipose stem/progenitor cells (ASCs) using transwell assay and found that IGF1 promoted cell migration in a dose dependent manner, with cytotactic effect peaking at 20 ng/mL (Fig. 4D–I).

Control-released IGF1 induced adipogenesis in vivo by homing endogenous stem/progenitor cells

A crucial challenge in novel approaches for the reconstruction of soft tissue defects, e.g. those from trauma or tumor resection, is survival of adipogenic cells in the graft and hence the maintenance of the volume of viable tissue volume [54]. Given that IGF1 stimulates adipose cell proliferation, migration and adipogenesis, especially by inducing a CD31-/34+/146− bias, we fabricated poly (lactic-co-glycolic acid) (PLGA) scaffolds (5×3 mm: dia.×height) to yield porosity for the homing of host endogenous cells and vasculature per our prior methods [55] (Fig. 5A, B). Microencapsulated IGF1 in PLGA spheres had an average ~100 to 500 μm pore size under SEM (Fig. 5C). IGF1 was control-released up to the tested 4 wks (Fig. 5D). IGF1-releasing microspheres in PLGA scaffolds were implanted in the inguinal fat pads of C57Bl6 mice *in vivo*, and retrieved after 4 wks (Fig. 5E), with IGF1-free, PLGA scaffolds as controls. The retrieved, representative IGF1 sample retained its original dimensions (5 mm dia.) (Fig. 5E). Little adipogenesis was observed in the representative scaffold with IGF1-free microspheres (Fig. 5F, G). Contrastingly, IGF1 delivery yielded robust adipogenesis (Fig. 5J, K), with adipose stroma and vasculature present (Fig. 5K). Quantitatively, IGF1 delivery yielded substantially more adipocytes and adipose tissue areas than sham controls (without IGF1) (Fig. 5N, O). FABP4 staining confirmed that lipid-laden cells in Fig. 5K were indeed adipocytes (Fig. 5L). Given no cells were transplanted in scaffolds, all tissues were formed by host endogenous cells that differentiated into adipocytes likely under the influence of IGF1 (Fig. 5K). Anti-CD146 antibody staining revealed both CD146+ and CD146− cells in samples with IGF1 delivery, while no obvious cells in IGF1 free samples (Fig. 5J, M). The appearance of CD146+ and

CD146− cells in the regenerated tissue might suggest that the above in vitro findings might be also true in vivo, which needs further study by cell tracing strategy.

IGF1 induced adipogenesis via Axin2/PPARγ pathways

In a follow-up experiment, we explored the underlying mechanisms for a putative crosstalk between PPARγ and Wnt/β-catenin in the context of CD31-/34+/146+/− cells and IGF1 promoted bias. Axin2 was selected given its role as a Wnt/β-catenin inhibitor and due to our observation that Wnt/β-catenin signaling was higher in CD31-/34+/146+ cells (Fig. 2). First, PPARγ was upregulated by IGF1 treatment in CD31-/34+ cells under adipogenesis induction medium, regardless of CD146 polarity (Fig. 6A). Similarly, we observed that IGF1 stimulated Axin2 expression in CD31-/34+ cells, regardless of CD146 positivity (Fig. 6B). Conversely, TOPflash luciferase activity and cyclin D1 were down-regulated upon IGF1 induction in CD31-/34+ cells (Fig. 6C, D), suggesting that IGF1 attenuates Wnt/β-catenin while in favor of Axin2 and PPARγ in adipogenesis.

Notably, Axin2 expression was significantly higher in native CD31-/34+/146− cells than that in CD31-/34+/146+ cells (in growth medium) (Fig. 6E). There was a linear correlation between Axin2 and PPARγ expression in both CD31-/34+/146− and in CD31-/34+/146+ cells (Fig. 6F), suggesting that PPARγ may transcriptionally activate Axin2. Forced expression of PPARγ and/or its co-activator PGC1α increased Axin2 expression at both protein and mRNA levels in growth medium (Fig. 6G, H), which remains true when cells cultured in adipogenesis induction medium (Fig. 6I). Conversely, siRNA knockdown of PPARγ and/or PGC1α (Fig. 6J–L) significantly attenuated Axin2 expression (Fig. 6M), suggesting that Axin2 might be a target of PPARγ and a mediator in the cross talk between Wnt of PPARγ.

We then identified a PPARγ response element (PPRE) in Axin2 promoter (Fig. 7A), indicating that PPARγ may transcriptionally activate Axin2. Furthermore, ChIP analysis revealed binding of PPARγ to Axin2 promoter region (Fig. 7B), suggesting perhaps a direct interaction between Axin2 promoter and PPARγ. A follow-up experiment showed that Axin2 luciferase reporter activity was significantly upregulated by PPARγ and/or PGC1α in the presence of the PPARγ response element (Fig. 7C). Conversely, PPRE deletion from the reporter abolished its response to PPARγ and/or PGC1α (Fig. 7D). To further confirm the role of Axin2 in adipogenesis, knockdown efficiency was achieved at both mRNA and protein levels of Axin2 by infection of lentivirus expressing shAxin2 (Fig. 7E, F). Axin2 knockdown increased TOPflash luciferase activity (Fig. 7G) and cyclin D1 expression (Fig. 7H), and reduced adipogenesis of SVF cells (Fig. 7I, J). Attenuated PPARγ expression with a time course of 0 to 14 days by Axin2 knockdown further confirmed Axin2's positive role in adipogenesis (Fig. 7K).

From the above data, we can see that IGF1 treatment resulted in increased PPARγ/Axin2 and decreased Wnt in both CD31-/34+/146+/− cells, with the fold change significantly higher in CD31-/34+/146+ cells. And the absolute levels become similar between the two types of cells (Fig. 6A–D). To this end, it is thus interesting to test whether IGF1 could reduce the difference between CD31-/34+/146+/− cells in adipogenesis and osteogenesis as observed in Fig. 1. We thus treated CD31-/34+/146+ cells and CD31-/34+/146− cells with

IGF1 and tested the adipogenesis and osteogenesis differences (Supplementary Fig. 4). As expected, the differences in adipogenesis between CD31-/34+/146+ cells and CD31-/34+/146− cells were very smaller (Supplementary Fig. 4A–D, I), which might be explained by the Wnt and PPARγ status (Fig. 6A–D). However, IGF1 treatment had no significant role on the osteogenesis of CD31-/34+/146− cells. And IGF1 treated CD31-/34+/146+ cells displayed slightly inhibited osteogenesis, which is consistent with previous findings that excess IGF1 inhibits osteogenesis [56] (Supplementary Fig. 4E–H, J). The osteogenesis between CD31-/34+/146+ cells and CD31-/34+/146− cells remained significantly different upon IGF1 treatment, which might be due to the regulatory role between IGF1 and Wnt/PPARγ was specific for adipogenesis (Fig. 6A–D).

A working schematic is proposed in Supplementary Fig. 1. IGF1 promotes a lineage bias towards CD31-/34+/146− cells from adipose stem/progenitor cells or the stromal vascular fraction of adipose tissue aspirates at the expense of CD31-/34+/146+ cells (Supplementary Fig. 1). However, IGF1 plays multifaceted roles in adipogenesis, not only inducing the proliferation of SVF cells, but also CD31-/34+ subpopulations regardless of CD146 polarity (Supplementary Fig. 1). Wnt/β-catenin pathway is innately robust in CD31-/34+/146+ cells and hence responsible for their modest adipogenesis capacity. Opposite to Wnt/β-catenin, innate CD31-/34+/146− cells have potent Axin2/PPARγ activity and when IGF1 stimulated, further enhance their adipogenic abilities that may be relevant to obesity and diabetes (Supplementary Fig. 1). Given IGF1's robust effects on inducing the migration of SVF cells that are present in adipose tissue, we showed adipogenesis in a sizable biomaterial scaffold by the homing of endogenous cells without cell transplantation (Figs. 5 **and** Supplementary Fig. 1). The presence of both CD146− and CD146+ cells in bioengineered adipose tissue suggests that IGF1 promoted CD31-/34+/146− bias might be true in the context of adipose tissue regeneration. Conversely, attenuation of IGF1/Axin2/PPARγ pathways may be effective approaches towards reducing obesity.

Discussion

The present findings represent an original discovery of two subpopulations of adipose stem cells with different rigor for adipogenesis. Adipose stem cells (ASCs) are broadly regarded as mononucleated and adherent cells isolated from the stromal vascular fraction of adipose tissue. Typically regarded ASCs are clearly heterogeneous [57, 58]. Previous work has shown that CD31-/34+ cells of the SVF are highly adipogenic [59]. Our finding of a novel CD31-/34+/146− subpopulation further indicates that multiple subpopulations of commonly regarded adipose stem cells are responsible for their adipogenic potential, perhaps in obesity and novel approaches of adipose regeneration. The location of CD31-/34+/146+/− cells is remarkable. CD31-/34+/146+ cells, as we showed here, are likely perivascular cells. However, CD31-/34+/146+ cells, likely due to their relatively innate high Wnt activity set, are not robust adipogenesis progenitors. Rapid proliferation of CD31-/34+/146+ cells in *ex vivo* culture suggests their capacity of expansion perhaps along blood vessels *in vivo*, consistent with previous findings on perivascular cells [60, 61]. Contrastingly, CD31-/34+/146− cells have slower proliferation rates and yet are robustly adipogenic, likely primary adipogenesis progenitors. Lineage tracing experiments in transgenic models will ascertain the stemness of CD31-/34+/146− cells. Polarizing abilities of CD31-/34+/146+ cells to

undergo osteogenic differentiation, and CD31-/34+/146− cells to undergo adipogenic differentiation indicated that adipose stroma harbors two separate progenitor populations: CD31-/34+/146+ cells with innate Wnt background and in homeostasis likely proliferate along with expanding blood vessels without inducing mineralization. Even if perivascularly localized CD31-/34+/146+ cells are progenitors of adipose tissue postnatally, they will need to exit the vascular wall and migrate into adipose stroma before differentiating into mature adipocytes and accumulating lipid vesicles, given that mature adipocytes are likely not able to migrate. CD31-/34+/146− cells are particularly remarkable in their ability to expand in adipose stroma directly and differentiate into adipocytes. CD31-/34+/146− cells reside in adipose stroma away from blood vessels, and therefore can readily differentiate into adipocytes.

Robust adipogenesis by CD31-/34+/146− cells might be due to the intrinsic higher expression of Axin2, a key Wnt signaling inhibitor that facilitates β-catenin phosphorylation and degradation. In contrast, higher β-catenin expression in CD31-/34+/146+ cells suggests a higher Wnt level that minimizes adipogenesis, partly in consistency with previous findings [62]. Notably, Axin2 regulation of adipogenesis appears to be universal, in SVF cells and CD31-/34+ fraction, regardless of CD146 polarity, analogous to adipogenic differentiation by Axin2 overexpression in 3T3-L1 preadipocytes[35]. Previously, Wnt has been shown to maintain preadipocytes in an undifferentiated state through inhibition of C/EBPa and PPARγ[35]. Knockdown of β-catenin abolishes adipogenesis inhibition [63]. The novel role of Axin2 in promoting adipogenesis appears to have broad implications in diabetes, obesity and reconstruction of soft tissue defects.

IGF1 has been previously found to promote adipogenesis and osteogenesis [64] but its proadipogenic mechanisms are evasive. We found that IGF1 has broad effects on adipose stem cells and their robust adipogenic fractions by promoting migration, proliferation and adipogenesis. IGF1 upregulates both Axin2 and PPARγ, and simultaneously attenuates Wnt/β-catenin under adipogenic conditions, leading to adipogenesis both in vitro and *in vivo* as shown here. Remarkably, IGF1 is responsible for a lineage switch from CD31-/34+/146+ cells to CD31-/34+/146− cells, in which Axin2/PPARγ pathways might be involved. Our data here suggest that CD146+ cells may depart from vascular wall and migrate into adipose stroma before further differentiating into mature adipocytes, which are worth for further confirmation. Loss of CD146 expression appears to be similar to a loss of CD24 expression[17], both ending with a net gain of adipogenesis capacity. As a departure from the common approach in adipose regeneration, we showed that a sizable (5×3 mm) adipose tissue formed in the inguinal fat pad by IGF1 mediated recruitment of endogenous cells. The appearance of both CD146− cells and CD146+ cells in the bioengineered adipose tissue suggests that certain host endogenous cells are recruited by IGF1, and further studies are needed to confirm the origin of these cells, for example, CD31-/34+/146+ cells. Similar to the regeneration of musculoskeletal tissues as we showed before[43], cytokine mediated cell homing may offer an alternative to cell transplantation approaches in tissue regeneration, including adipose tissue. Conversely, attenuation of entry of adipose stem/progenitor cells towards CD31-/34+/146− cells may be effective in reducing obesity.

Methods

Adipose tissue sampling and cell isolation

Following IRB approval, human adipose tissue was collected from an anonymous donor (female; 52 years old; no personal identifier) who underwent elective lipectomy at Columbia University Medical Center. Additional *in vitro* experiments were conducted on adipose tissue samples of six other female patients (age range: 35 to 57; average 44 years). Detailed information is provided in Supplementary Table 1. The stromal vascular fraction (SVF) of adipose tissue, commonly known as adipose stem/progenitor cells (ASCs), were isolated as mononucleated adherent cells using published protocols and our prior work [65–67]. Briefly, lipoaspirate was digested for 30 min in 0.1% collagenase I (Sigma, St. Louis, Mo) at 37°C. The resulting suspension was filtered with a 100-μm filter and centrifuged at 2000 g. The resulting cell pellet was resuspended in 160-mM ammonium chloride buffer to lyse red blood cells and again centrifuged at 2000 g. The new cell pellet was resuspended in MesenPRO RS™ Medium (Invitrogen, Carlsbad, CA) and passed through a 40-mm cell strainer. The isolated cells were plated at 37°C and 5% CO_2. Following removal of non-adherent cells in 48 hrs, mononucleated and adherent cells were passaged at 70% confluence, with medium change every 3–4 days.

Immunofluorescent analysis of adipose tissue and cells

Freshly harvested adipose tissue was washed in PBS, 7.5% gelatin, 15% sucrose (Sigma), before freezing in liquid nitrogen-cooled 2-methylbutane (Fisher Scientific, Fair Lawn, NJ). Sections (8 μm) were cut on a cryostat, fixed for 5 min in acetone and stored at −80°C. Before staining, sections were dried and post-fixed for 30 min in 10% formalin. Tissue was rehydrated and washed in PBS. Tissue sections were pretreated for 1 h at room temperature with protein block solution (Dako, Carpinteria, CA) to prevent nonspecific binding. Slides were then incubated with rabbit anti-CD146 (1:100, #ab75769, Abcam) together with goat anti-CD31 (1:100, #sc-1506 –R, Santa Cruz, Santa Cruz, CA) and/or with mouse anti-CD34 (1:100, #ab8536, Abcam) overnight at 4°C, followed by washing and incubation with secondary antibodies, goat anti-rabbit Alexa 594 and goat anti-mouse Alexa 488 antibodies. Nuclear staining was attained with 6-diamidino-2-phenylindole (DAPI, Invitrogen). For staining of sorted cells, freshly sorted CD31-CD34+CD146+/− cells were cultured until 70–80% confluence. Following protein blocking, cells were incubated with primary mouse anti-Ki67 (1:1000, # ab16667, Abcam) and β-catenin (1:1000, #ab6302, Abcam) with positive and negative controls, per our prior methods [68].

Flow cytometry and cell sorting

Passage 1 to 3 SVF cells were incubated simultaneously with monoclonal mouse anti-human fluorochrome-conjugated antibodies, CD31-Alexa 488 (5 μl for 1×10^6 cells, #558068, BD, Biosciences, San Jose, CA), CD34-allophycocyanin (APC, 5 μl for 1×10^6 cells, #561209, BD) and CD146-phycoerythrin (PE, 20 μl for 1×10^6 cells, #550315, BD). Cell sorting was performed using a three-laser Mo-Flo High-Speed Cell Sorter. Spectral overlap compensation was manually achieved prior to cell sorting for each fluorescence parameter for single fluorochromatic molecules (FITC, PE, and APC). CD31-CD34− and CD31-CD34+CD146+/− cells were collected into chilled sterile polypropylene tubes.

Cell proliferation and adipogenic differentiation

Sorted CD31-CD34+CD146+/− cells were seeded in 96-well plates at a density of 2×10^3 cells per well. Cell Counting Kit-8 (CCK-8) solution was used to measure cellularity with 450-nm absorbance. Sorted cells were seeded at 80% confluence and cultured with MesenPRO RS™ Medium until near confluence. Growth media were replaced with adipogenic differentiation media (#A1007001, Invitrogen), with medium change every 2 days. RNA samples were collected at days 0, 7, 14 and 21. For Oil red O staining, cells were washed with PBS, fixed with 10% formaldehyde and stained with Oil red O solution for 10 min.

Migration assay

Cell migration was measured using Transwell with 8-μm pore inserts (Falcon/Becton Dickinson). Briefly, following culture in serum-free medium for 24 hrs, 50,000 SVF cells in serum-free medium were seeded in Transwell inserts and subjected to different IGF1 concentrations (R&D). Unmigrated cells in the upper chamber of the insert were removed, and cell migration in the lower chamber of the insert was assessed by violet staining after 12 h.

RNA extraction and qPCR

Total RNA was isolated using Trizol (#15596018, Invitrogen) and used for complementary DNA synthesis. cDNA synthesis was done with random hexamer primers using SuperScript® III First-Strand Synthesis SuperMix (Invitrogen). mRNA expression was measured by quantitative real-time PCR (TaqMan), with targeted mRNA expression normalized to GAPDH or β-actin.

Western blot

Cells were washed with ice-cold PBS and extracted in lysis buffer with protease/phosphatase inhibitor cocktail (Thermo Scientific). Proteins were separated on an 8–12% SDS-PAGE, transferred to nitrocellulose membranes, and detected with goat monoclonal anti-GAPDH, rabbit polyclonal anti-Axin2 (1:1000, #ab32197, Abcam), mouse monoclonal anti-PPARγ (1:1000, #ab70405, Abcam), rabbit polyclonal anti-PGC1 (1:1000, #ab191838, Abcam) or rabbit monoclonal anti-β-catenin (1:1000, #ab 32572, Abcam).

Chromatin immunoprecipitation assay (ChIP assay)

ChIP assay was done with Imprint® Chromatin Immunoprecipitation Kit (Sigma). Briefly, ASCs (1×10^7 cells/sample) were cross-linked and quenched with ice-cold 1.25 M glycine. Cross-linked cells were resuspended, and lysed to separate the nuclear pellet. The nucleic was pelleted and resuspended in 500 μl Shearing Buffer containing protease inhibitor cocktail, and sonicated to shear the cross-linked DNA to an optimal fragment size ranging from 200 to 1000 bp. Sonication was performed using a sonic dismembrator (Power 4.5 for 30W) for twenty rounds of 15-second pulses (with a 45-second pause between pulses). Simultaneously, Stripwells were incubated with 1 μl polyclonal antibody against PPARγ (Santa Cruz) or 1 μl Normal Mouse IgG control in 100μl Antibody Buffer for 2 hrs at room temperature. Sonicated chromatin was further diluted with same volume of Dilution buffer,

and 5 μl of the sonicated nuclear pellet was set aside on ice as Input and then taken through the rest of the protocol exactly as the immunoprecipitated (IP) fraction. The rest of sonication sample (about 100 μl) combined with the preincubated beads and this immunoprecipitation was incubated at room temperature for 2 hrs on an orbital shaker. The incubated wells were washed with IP Wash Buffer. Bound DNA-protein complexes were eluted from the beads by reversal of crosslinking through incubating with Reversing Solution at 4°C overnight. The ChIP lysate was mixed with 400 μl Binding Solution, and collected after 3 times flow through and centrifugation. The final DNA was resuspended with 25 μl Elution Solution. ChIP PCR primers were: β-actin: Forward, GTGGTCCTGCGACTTCTAATG; Reverse, TGCCGACTTCAGAGCAACTGC. Axin2: Forward, GATGAAAGTCTCCCCTGAGTGAG; Reverse, GCGCTCCCTCTTCCCACTCC.

Plasmids, transfection and luciferase assay

1kb Axin2 promoter reporter, TOPflash reporter, PGC1α, PPARγ expression vector, and control EGFP were from Addgene. The internal control vector pGL4.73 [hRluc/SV40] was from Promega. siRNA against PGC1α (#ASO0W515), PPARγ (#ASO0W516), and Axin2 (#ASO0WAZI) and the negative control (#AM4642) were obtained from Ambion. For plasmid transfection, electroporation was performed (Invitrogen). For siRNA transfection, siRNA duplexes were transfected with lipofectamine 2000. To generate reporter construct without the predicted PPRE, the fragment without the PPRE was amplified using the primer set: Forward, CCGGGCTAGCCAAGTCAGCAGGGGC, and Reverse, CCGGTACCGGGAGGAGTGGGAAGACAGAGGTG. Then the amplified fragment was cloned into pGL3-basic vector using the Nhe1 and Xho1 sites. To conduct the luciferase assay, cells were seeded in 24-well plates (Corning) at a density of 2×10^5 cells per well one day before transfection. Reporter constructs and overexpression vectors or siRNAs were co-transfected at indicated concentrations using Lipofectamine® 2000 per manufacturer's protocol (Invitrogen). After 48 hrs, firefly and Renilla luciferase activities were measured with Dual-Glo luciferase assay system per manufacturer's instructions (Promega).

Lentivirus production and transfection

Scrambled shRNA or shAxin2 (4 μg), VSVG (4 μg) and Δ8.9 (0.8 μg) vectors were co-transfected into 80% confluent 293T cells using lipofectamine 2000 per manufacturer's protocol (Invitrogen). Virus supernatant was collected 2 days after transfection and filtered with 0.45 μm membrane. SVF cells were cultured to 30–50% confluence and infected with lentivirus in 4 μg/mL polybrene (Santa Cruz). Infected cells were selected with Puromycin and exposed to adipogenesis differentiation medium.

Scaffold microsphere fabrication

Poly (lactic-co-glycolic acid) copolymer scaffolds were fabricated per our prior work [69, 70]. Briefly, NaCl crystals were sieved to obtain crystals in the range of 125–500 μm. 3 g of 85:15 PLGA (Sigma Aldrich) was dissolved in 30-mL DCM and the solution was poured over 27 g of sieved NaCl and left to dry overnight. Following solvent evaporation, 5-mm diameter discs were punched out. The discs were freeze-dried and stored at −20°C. Pore size was analyzed using scanning electron microscopy. PLGA microspheres were prepared per

our prior methods [55] using double emulsion (water-in-oil in water). Briefly, 250-mg, 50:50 PLGA (Sigma Aldrich) was dissolved in 1-mL dichloromethane (DCM). IGF1 encapsulation and release were measured per our prior methods [71], with dissolving 10-mg IGF1 in 50-μl PBS and added to the DCM, which was vortexed and transferred to 0.1% PVA solution and stirred for 2 hrs. The microspheres were washed in distilled water and freeze-dried, and then stored at −20°C. All scaffolds were sterilized in the ethanol for 30 min before *in vivo* transplantation.

In vivo scaffold transplantation

Under IACUC approval, C57Bl6 mice were kept on a high fat diet for six weeks to ensure sufficient abdominal fat mass for implantation of PLGA scaffolds prior to surgery. The mice were anesthetized using isoflurane. The fur was removed, followed by disinfection with betadine and ethanol. A 2-cm skin incision was made in the lower abdominal region. An incision was made in the inguinal fat pad followed by insertion of IGF1 loaded PLGA scaffolds, with IGF1-free empty microsphere in PLGA scaffolds as controls. Extra care was taken to ensure that the scaffolds were completely surrounded by adipose tissue. The wound was suture-closed. After four weeks, all scaffolds were retrieved by carefully removing surrounding inguinal adipose tissue, and immersed in formalin for overnight fixation, followed by sectioning and staining with hematoxylin and eosin, with additional sections for immunohistochemistry.

Immunohistochemistry

Sections were deparaffinized, rehydrated in graded ethanol, boiled in citrate buffer for antigen retrieval, and stained with a primary antibody for FABP4 (1:200, #ab13979, Abcam, Cambridge, UK) and CD146 (1:200, #ab75769, Abcam). HRP-conjugated secondary antibody (#87–8963, Invitrogen) was used (#00–1111, Invitrogen).

Statistical analysis

All experiments were performed at least three times, and all quantitative data were analyzed by Student's *t-test* or one-way ANOVA with Bonferroni corrections upon confirmation of normal data distribution, with significance of $p \leq 0.05$.

Supplementary Material

Refer to Web version on PubMed Central for supplementary material.

Acknowledgments

We thank Ms. Q. Guo and Ms. J. Melendez for administrative and technical assistance. The effort for composition of this article is supported by NIH grants R01AR065023 and R01DE023112 to J.J. Mao.

References

1. Spiegelman BM, Flier JS. Adipogenesis and obesity: rounding out the big picture. Cell. 1996; 87(3): 377–89. [PubMed: 8898192]
2. Rosen ED, Spiegelman BM. What we talk about when we talk about fat. Cell. 2014; 156(1–2):20–44. [PubMed: 24439368]

3. Cohen P, et al. Ablation of PRDM16 and beige adipose causes metabolic dysfunction and a subcutaneous to visceral fat switch. Cell. 2014; 156(1–2):304–16. [PubMed: 24439384]
4. Schmidt BA, Horsley V. Intradermal adipocytes mediate fibroblast recruitment during skin wound healing. Development. 2013; 140(7):1517–27. [PubMed: 23482487]
5. Astori G, et al. "In vitro" and multicolor phenotypic characterization of cell subpopulations identified in fresh human adipose tissue stromal vascular fraction and in the derived mesenchymal stem cells. J Transl Med. 2007; 5:55. [PubMed: 17974012]
6. Balwierz A, et al. Human adipose tissue stromal vascular fraction cells differentiate depending on distinct types of media. Cell Prolif. 2008; 41(3):441–59. [PubMed: 18422701]
7. Zimmerlin L, et al. Stromal vascular progenitors in adult human adipose tissue. Cytometry A. 2010; 77(1):22–30. [PubMed: 19852056]
8. Hager G, et al. Three specific antigens to isolate endothelial progenitor cells from human liposuction material. Cytotherapy. 2013; 15(11):1426–35. [PubMed: 24094492]
9. Yoshimura K, et al. Characterization of freshly isolated and cultured cells derived from the fatty and fluid portions of liposuction aspirates. J Cell Physiol. 2006; 208(1):64–76. [PubMed: 16557516]
10. Maumus M, et al. Native human adipose stromal cells: localization, morphology and phenotype. Int J Obes (Lond). 2011; 35(9):1141–53. [PubMed: 21266947]
11. Gronthos S, et al. Surface protein characterization of human adipose tissue-derived stromal cells. J Cell Physiol. 2001; 189(1):54–63. [PubMed: 11573204]
12. Wickham MQ, et al. Multipotent stromal cells derived from the infrapatellar fat pad of the knee. Clin Orthop Relat Res. 2003; 412:196–212. [PubMed: 12838072]
13. Guilak F, et al. Clonal analysis of the differentiation potential of human adipose-derived adult stem cells. J Cell Physiol. 2006; 206(1):229–37. [PubMed: 16021633]
14. Li H, et al. Adipogenic potential of adipose stem cell subpopulations. Plast Reconstr Surg. 2011; 128(3):663–72. [PubMed: 21572381]
15. Sengenes C, et al. Preadipocytes in the human subcutaneous adipose tissue display distinct features from the adult mesenchymal and hematopoietic stem cells. J Cell Physiol. 2005; 205(1):114–22. [PubMed: 15880450]
16. Rodeheffer MS, Birsoy K, Friedman JM. Identification of white adipocyte progenitor cells in vivo. Cell. 2008; 135(2):240–9. [PubMed: 18835024]
17. Berry R, Rodeheffer MS. Characterization of the adipocyte cellular lineage in vivo. Nat Cell Biol. 2013; 15(3):302–8. [PubMed: 23434825]
18. Eguchi J, et al. Interferon regulatory factors are transcriptional regulators of adipogenesis. Cell Metab. 2008; 7(1):86–94. [PubMed: 18177728]
19. Wu Z, Puigserver P, Spiegelman BM. Transcriptional activation of adipogenesis. Curr Opin Cell Biol. 1999; 11(6):689–94. [PubMed: 10600710]
20. Rosen ED, et al. Transcriptional regulation of adipogenesis. Genes Dev. 2000; 14(11):1293–307. [PubMed: 10837022]
21. Chen Z, et al. Krox20 stimulates adipogenesis via C/EBPbeta-dependent and -independent mechanisms. Cell Metab. 2005; 1(2):93–106. [PubMed: 16054051]
22. Birsoy K, Chen Z, Friedman J. Transcriptional regulation of adipogenesis by KLF4. Cell Metab. 2008; 7(4):339–47. [PubMed: 18396140]
23. Rivero S, et al. DLK2 is a transcriptional target of KLF4 in the early stages of adipogenesis. J Mol Biol. 2012; 417(1–2):36–50. [PubMed: 22306741]
24. Freytag SO, Geddes TJ. Reciprocal regulation of adipogenesis by Myc and C/EBP alpha. Science. 1992; 256(5055):379–82. [PubMed: 1566086]
25. Zuo Y, Qiang L, Farmer SR. Activation of CCAAT/enhancer-binding protein (C/EBP) alpha expression by C/EBP beta during adipogenesis requires a peroxisome proliferator-activated receptor-gamma-associated repression of HDAC1 at the C/ebp alpha gene promoter. J Biol Chem. 2006; 281(12):7960–7. [PubMed: 16431920]
26. Payne VA, et al. C/EBP transcription factors regulate SREBP1c gene expression during adipogenesis. Biochem J. 2010; 425(1):215–23. [PubMed: 19811452]

27. Gervois P, Fruchart JC. PPAR gamma: a major nuclear receptor in adipogenesis. Med Sci (Paris). 2003; 19(1):20–2. [PubMed: 12836187]
28. Ge K, et al. Transcription coactivator TRAP220 is required for PPAR gamma 2-stimulated adipogenesis. Nature. 2002; 417(6888):563–7. [PubMed: 12037571]
29. Cipolletta D, et al. PPAR-gamma is a major driver of the accumulation and phenotype of adipose tissue Treg cells. Nature. 2012; 486(7404):549–53. [PubMed: 22722857]
30. Tontonoz P, Hu E, Spiegelman BM. Stimulation of adipogenesis in fibroblasts by PPAR gamma 2, a lipid-activated transcription factor. Cell. 1994; 79(7):1147–56. [PubMed: 8001151]
31. Huang Y, et al. gamma-secretase inhibitor induces adipogenesis of adipose-derived stem cells by regulation of Notch and PPAR-gamma. Cell Prolif. 2010; 43(2):147–56. [PubMed: 20447060]
32. Lim X, Nusse R. Wnt signaling in skin development, homeostasis, and disease. Cold Spring Harb Perspect Biol. 2013; 5(2)
33. Clevers H. Wnt/beta-catenin signaling in development and disease. Cell. 2006; 127(3):469–80. [PubMed: 17081971]
34. Yang Y. Wnt signaling in development and disease. Cell Biosci. 2012; 2(1):14. [PubMed: 22520685]
35. Ross SE, et al. Inhibition of adipogenesis by Wnt signaling. Science. 2000; 289(5481):950–3. [PubMed: 10937998]
36. Keats EC, et al. Switch from canonical to noncanonical Wnt signaling mediates high glucose-induced adipogenesis. Stem Cells. 2014
37. Chung SS, et al. Regulation of Wnt/beta-catenin signaling by CCAAT/enhancer binding protein beta during adipogenesis. Obesity (Silver Spring). 2012; 20(3):482–7. [PubMed: 21760632]
38. Christodoulides C, et al. Adipogenesis and WNT signalling. Trends Endocrinol Metab. 2009; 20(1):16–24. [PubMed: 19008118]
39. Takada I, et al. A histone lysine methyltransferase activated by non-canonical Wnt signalling suppresses PPAR-gamma transactivation. Nat Cell Biol. 2007; 9(11):1273–85. [PubMed: 17952062]
40. Takada I, Kouzmenko AP, Kato S. Wnt and PPARgamma signaling in osteoblastogenesis and adipogenesis. Nat Rev Rheumatol. 2009; 5(8):442–7. [PubMed: 19581903]
41. Zeve D, et al. Wnt signaling activation in adipose progenitors promotes insulin-independent muscle glucose uptake. Cell Metab. 2012; 15(4):492–504. [PubMed: 22482731]
42. Scholtysek C, et al. PPARbeta/delta governs Wnt signaling and bone turnover. Nat Med. 2013; 19(5):608–13. [PubMed: 23542786]
43. Lee CH, et al. Regeneration of the articular surface of the rabbit synovial joint by cell homing: a proof of concept study. Lancet. 2010; 376(9739):440–8. [PubMed: 20692530]
44. Zuk PA, et al. Human adipose tissue is a source of multipotent stem cells. Mol Biol Cell. 2002; 13(12):4279–95. [PubMed: 12475952]
45. Mitterberger MC, et al. DLK1(PREF1) is a negative regulator of adipogenesis in CD105(+)/CD90(+)/CD34(+)/CD31(-)/FABP4(-) adipose-derived stromal cells from subcutaneous abdominal fat pats of adult women. Stem Cell Res. 2012; 9(1):35–48. [PubMed: 22640926]
46. Lv FJ, et al. The surface markers and identity of human mesenchymal stem cells. Stem Cells. 2014
47. Corselli M, et al. Perivascular support of human hematopoietic stem/progenitor cells. Blood. 2013; 121(15):2891–901. [PubMed: 23412095]
48. Crisan M, et al. Perivascular cells for regenerative medicine. J Cell Mol Med. 2012; 16(12):2851–60. [PubMed: 22882758]
49. Lin CS, et al. Is CD34 truly a negative marker for mesenchymal stromal cells? Cytotherapy. 2012; 14(10):1159–63. [PubMed: 23066784]
50. Maddox JR, et al. Effects of Culturing on the Stability of the Putative Murine Adipose Derived Stem Cells Markers. Open Stem Cell J. 2009; 1:54–61. [PubMed: 19946473]
51. Braun J, et al. Concerted regulation of CD34 and CD105 accompanies mesenchymal stromal cell derivation from human adventitial stromal cell. Stem Cells Dev. 2013; 22(5):815–27. [PubMed: 23072708]

52. Laudes M. Role of WNT signalling in the determination of human mesenchymal stem cells into preadipocytes. J Mol Endocrinol. 2011; 46(2):R65–72. [PubMed: 21247979]
53. Scavo LM, et al. Insulin-like growth factor-I stimulates both cell growth and lipogenesis during differentiation of human mesenchymal stem cells into adipocytes. J Clin Endocrinol Metab. 2004; 89(7):3543–53. [PubMed: 15240644]
54. Stosich MS, et al. Bioengineering strategies to generate vascularized soft tissue grafts with sustained shape. Methods. 2009; 47(2):116–21. [PubMed: 18952179]
55. Moioli EK, et al. Sustained release of TGFbeta3 from PLGA microspheres and its effect on early osteogenic differentiation of human mesenchymal stem cells. Tissue Eng. 2006; 12(3):537–46. [PubMed: 16579687]
56. Huang Z, et al. Modulating osteogenesis of mesenchymal stem cells by modifying growth factor availability. Cytokine. 2010; 51(3):305–10. [PubMed: 20580248]
57. Gimble J, Guilak F. Adipose-derived adult stem cells: isolation, characterization, and differentiation potential. Cytotherapy. 2003; 5(5):362–9. [PubMed: 14578098]
58. Gimble JM, et al. Concise review: Adipose-derived stromal vascular fraction cells and stem cells: let's not get lost in translation. Stem Cells. 2011; 29(5):749–54. [PubMed: 21433220]
59. Zuk PA, et al. Multilineage cells from human adipose tissue: implications for cell-based therapies. Tissue Eng. 2001; 7(2):211–28. [PubMed: 11304456]
60. Zimmerlin L, et al. Mesenchymal markers on human adipose stem/progenitor cells. Cytometry A. 2013; 83(1):134–40. [PubMed: 23184564]
61. Jumabay M, et al. Endothelial differentiation in multipotent cells derived from mouse and human white mature adipocytes. J Mol Cell Cardiol. 2012; 53(6):790–800. [PubMed: 22999861]
62. Li HX, et al. Roles of Wnt/beta-catenin signaling in adipogenic differentiation potential of adipose-derived mesenchymal stem cells. Mol Cell Endocrinol. 2008; 291(1–2):116–24. [PubMed: 18584948]
63. Cawthorn WP, et al. Wnt6, Wnt10a and Wnt10b inhibit adipogenesis and stimulate osteoblastogenesis through a beta-catenin-dependent mechanism. Bone. 2012; 50(2):477–89. [PubMed: 21872687]
64. Xue P, et al. IGF1 promotes osteogenic differentiation of mesenchymal stem cells derived from rat bone marrow by increasing TAZ expression. Biochem Biophys Res Commun. 2013; 433(2):226–31. [PubMed: 23473758]
65. Alhadlaq A, Tang M, Mao JJ. Engineered adipose tissue from human mesenchymal stem cells maintains predefined shape and dimension: implications in soft tissue augmentation and reconstruction. Tissue Eng. 2005; 11(3–4):556–66. [PubMed: 15869434]
66. Hu L, et al. Side-by-side comparison of the biological characteristics of human umbilical cord and adipose tissue-derived mesenchymal stem cells. Biomed Res Int. 2013; 2013:438243. [PubMed: 23936800]
67. Zhao J, et al. The effects of cytokines in adipose stem cell-conditioned medium on the migration and proliferation of skin fibroblasts in vitro. Biomed Res Int. 2013; 2013:578479. [PubMed: 24416724]
68. Lee CH, et al. CTGF directs fibroblast differentiation from human mesenchymal stem/stromal cells and defines connective tissue healing in a rodent injury model. J Clin Invest. 2010; 120(9):3340–9. [PubMed: 20679726]
69. Patrick CW Jr, et al. Preadipocyte seeded PLGA scaffolds for adipose tissue engineering. Tissue Eng. 1999; 5(2):139–51. [PubMed: 10358221]
70. Pattison MA, et al. Three-dimensional, nano-structured PLGA scaffolds for bladder tissue replacement applications. Biomaterials. 2005; 26(15):2491–500. [PubMed: 15585251]
71. Kilic A, et al. Effect of white adipose tissue flap and insulin-like growth factor-1 on nerve regeneration in rats. Microsurgery. 2013; 33(5):367–75. [PubMed: 23653396]

Significance Statement

Adipogenesis is relevant to obesity, diabetes and surgical reconstruction following trauma or tumor resection. We discovered a specific fraction of stem cells in human fat tissue that have strong ability to become adipose cells, and yet another fraction with strong ability to become bone. Two molecular signaling pathways regulate the yin and yang of adipose stem cells to become bone or fat tissue. We then discovered that a recombinant human protein induced the formation of sizable adipose tissue in a way that may help reconstruct soft tissue defects due to trauma, infectious diseases or tumor resections.

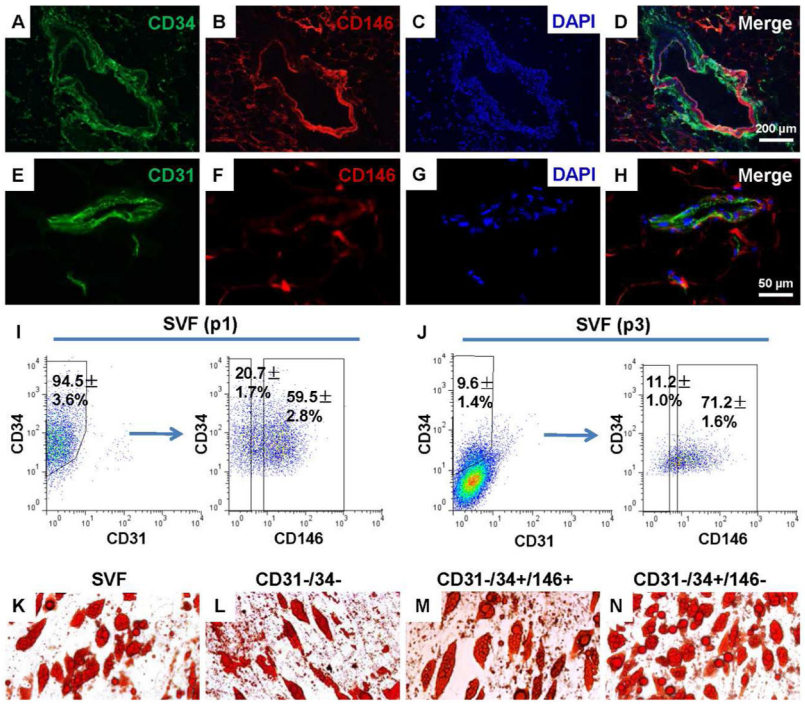

Figure 1. Immunolocalization of CD31-/34+/146+/− cells in lipectomized human adipose tissue and adipogenic fractions

Sections of human adipose tissue (anonymous female, 52-yrs-old) were stained with anti-CD34 **(A)**, anti-CD146 **(B, F)** and counterstained with DAPI **(C, G)**. Merged image shows that CD146+ cells were primarily, but not exclusively, associated with blood vessels **(D)**. CD31 **(E)** was virtually exclusively associated with blood vessels. Again, not all CD146+ cells were associated with blood vessels in the merged image **(H)** (a–d, scale bar, 200 μm; e–h, scale bar, 50 μm). **(I)** Flow cytometry showed that ~94.5% cells in the first passage of the stromal vascular fraction (SVF p1) of this lipectomized human adipose tissue were CD31-/34+, among which ~20.7% were CD146−, and ~59.5% were CD146+. By the third passage (SVF p3) **(J)**, CD31-/34+ cells dropped drastically from ~94.5% to 9.6%. There was a lineage reduction of CD146− cells from ~20.7% to ~11.2% with a concomitant gain of 146+ cells (from ~59.2% to ~71.2%) (mean ± s.d., n=3). Adipogenesis occurred when SVF cells **(K)**, CD31-/34− cells **(L)** and CD31-/34+/146+/− cells **(M, N)** were exposed to adipogenic medium. Strikingly, CD31-/34+/146− cells showed remarkable adipogenesis ability **(N)** with corresponding quantitative data of PPARγ and FABP4 expression **(O)** (mean ± s.d., n=3, **p<0.01, ANOVA); (scale bar, 200 μm for K–N). Ki67 showed rapid proliferation of CD31-/34+/146+ cells **(P)**, relative to CD31-/34+/146− cells **(Q)** (scale bar, 50 μm) with quantitative data of Ki67 positive cells percentage (**R**). Osteogenic potential (Alizarin red) of SVF cells (**S**), CD31-/34− cells (**T**), CD31-/34+/146+ cells (**U**) and CD31-/34+/146− cells (**V**).

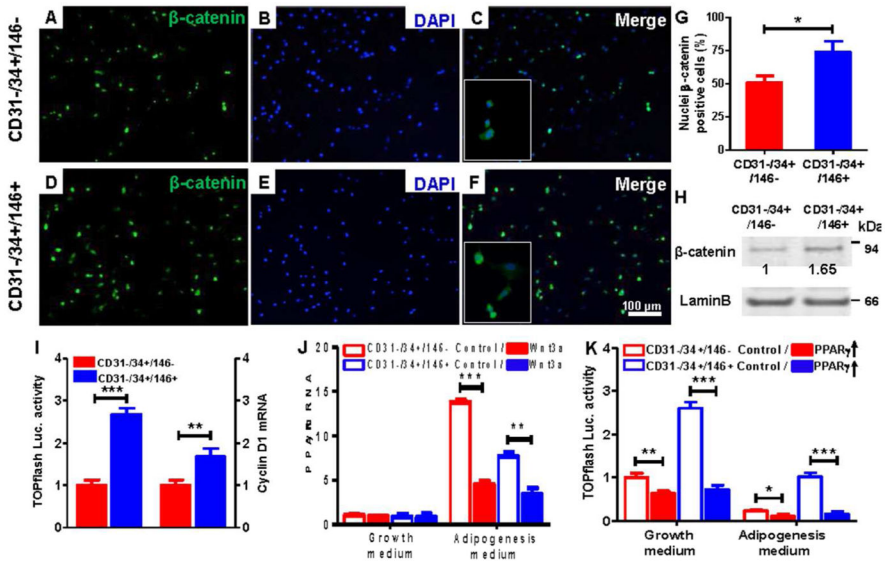

Figure 2. Contrasting Wnt and PPARγ signaling in CD31-CD34+CD146− and CD31-CD34+CD146+ cells

β-catenin staining was modest in CD31-/34+/146− cells **(A, B, C** and **insert)**. CD31-CD34+CD146+ cells showed robust nuclear β-catenin staining **(D, E, F** and **insert)** (scale bar, 100 μm). Nuclei β-catenin positive cells were quantitatively detected (**G**) (mean ± s.d., n=3, *p<0.05, Student's t-test), and β-catenin protein level was pronounced in CD31-/34+/146+ cells, relative to CD31-/34+CD146− cells **(H)**. Wnt Topflash activity and cyclin D1 were significantly higher in CD31-/34+/146+ cells than CD31-/34+/146− cells **(I)** (mean ± s.d., n=3, **p<0.01, ***p<0.001, ANOVA). PPARγ was significantly attenuated after CD31-/34+ cells, regardless of CD146 polarity, were exposed to with 10 ng/mL Wnt3a in adipogenesis medium **(J)**. Conversely, PPARγ overexpression in CD31-/34+ cells, regardless of CD146 polarity, was associated with attenuated Wnt topflash activity **(K)** (mean ± s.d., n=3, **p<0.01, ***p<0.001, ANOVA).

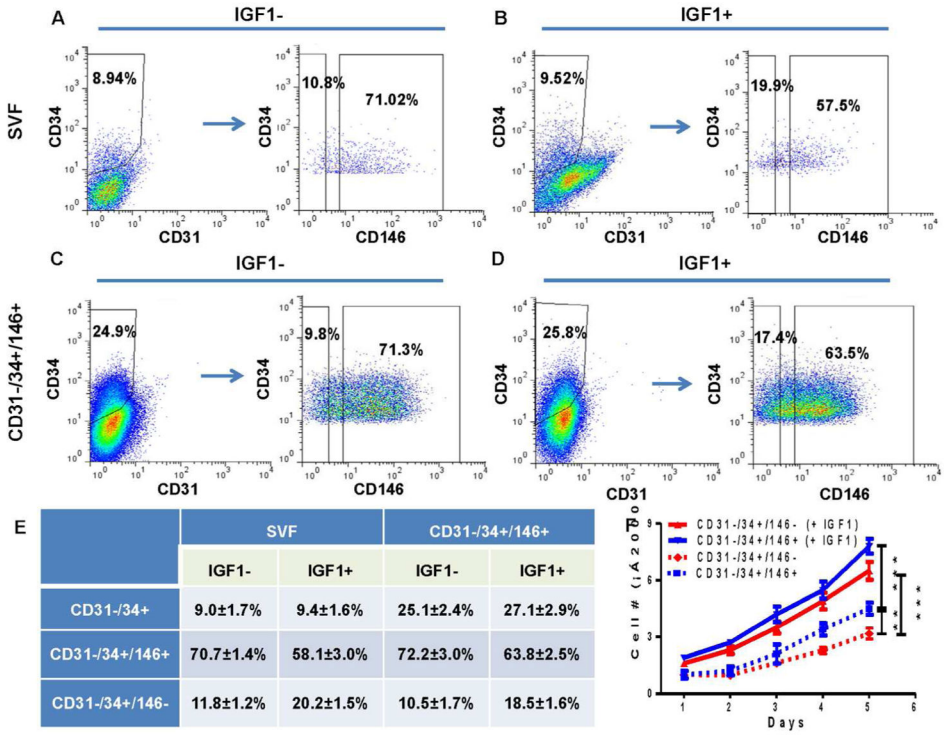

Figure 3. IGF1 enriches CD31-CD34+CD146− subpopulation

The third passage of stromal vascular fraction of human adipose stem/progenitor cells was subjected to flow cytometry **(A)**. With 10 ng/mL IGF1, CD31-/34+CD146− cells increased from ~10.8% to ~19.9%, whereas CD31-/34+/146+ cells decreased from ~71.02% to ~57.5% **(A, B)**. IGF1 stimulated a lineage bias of CD31-/34+ subpopulation towards CD146− cells **(C, D)**. The lineage switch towards CD146− cells did not affect the totality of CD31-/34+ cells **(E)** (mean ± s.d., n=3; ANOVA). CD31-/34+/146+ cells showed significantly higher proliferation rates than donor-matched CD31-/34+/146− cells **(F)**. IGF1 further increased the proliferation rates of CD31-/34+ cells, regardless of CD146 polarity, by maintaining the same trend with significantly greater proliferation rates of CD31-/34+/146+ cells **(F)** (mean ± s.d., n=3, **p<0.01, ***p<0.001, ANOVA).

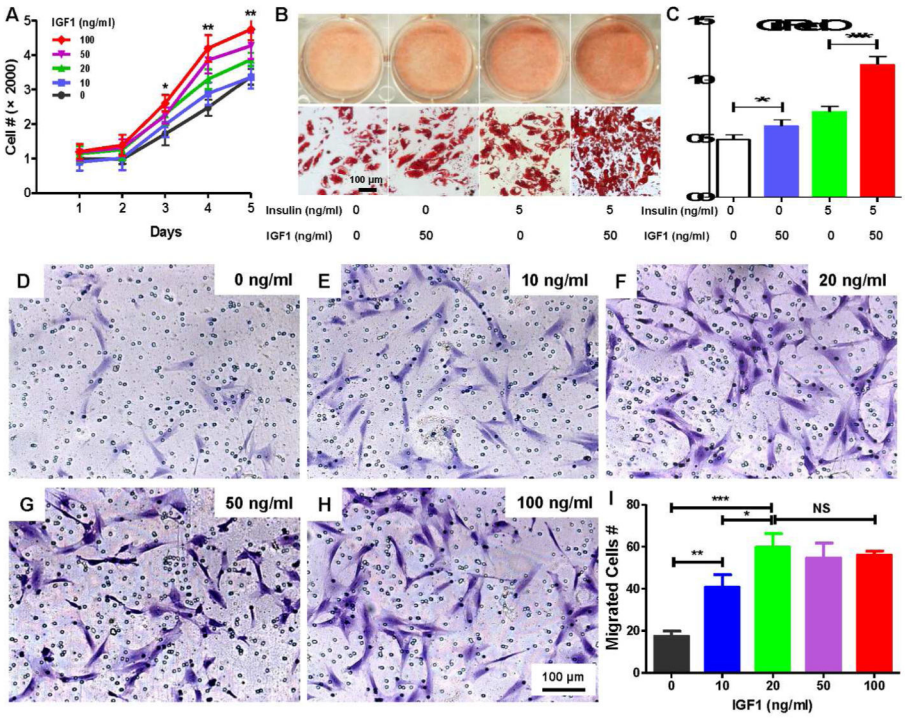

Figure 4. IGF1 promotes proliferation, adipogenic differentiation and migration

IGF1 (0–100 ng/mL) promoted the proliferation of stromal vascular fraction (SVF) cells from lipectomized human adipose tissue in a dose dependent manner **(A)** (mean ± s.d., n=3, *p<0.05, **p<0.01, ANOVA). IGF1 promoted adipogenesis upon 14-day induction in chemically defined medium, prominently in the presence of insulin; Oil red O staining **(B)** (scale bar, 100 μm), with quantification in **C**, showing 50 ng/mL IGF1 induced significant adipogenesis **(C)** (mean ± s.d., n=3, *p<0.05, ***p<0.001, ANOVA). **(D–H)** Different numbers of SVF cells from lipectomized human adipose tissue migrated (Crystal violet staining) (scale bar, 100 μm), with quantified data in **(I)** (mean ± s.d., n=3, *p<0.05, **p<0.01, ***p<0.001, ANOVA, NS: no significance).

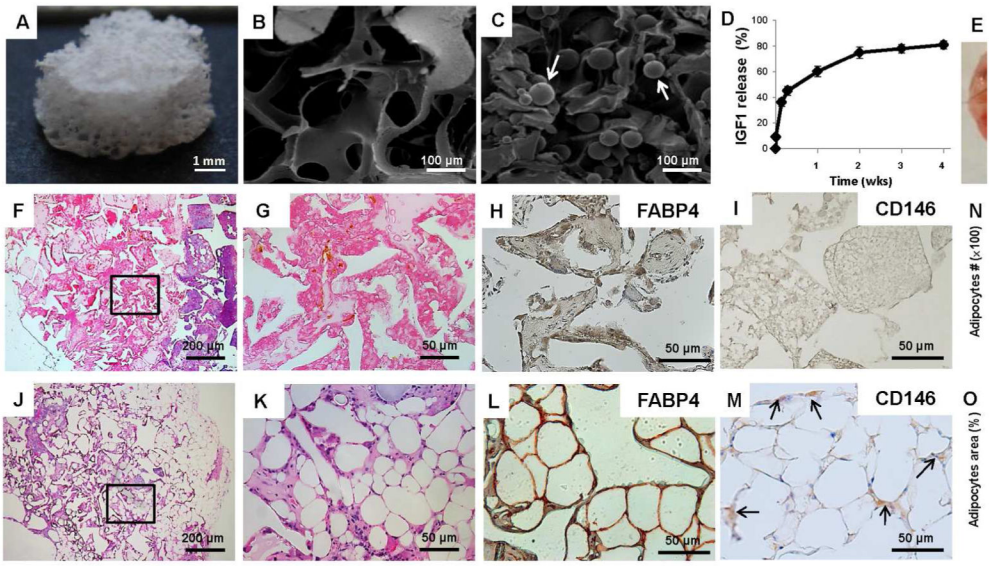

Figure 5. Control-released IGF1 induces *in vivo* adipogenesis

Porous poly (lactic-co-glycolic acid) (PLGA) scaffolds (5×3 mm) **(A)** were fabricated with pore size range of 125 to 500 μm (SEM) **(B)**. SEM of a bisected PLGA scaffold to reveal loaded PLGA microspheres (arrows) **(C)**. IGF1 was encapsulated in PLGA microspheres and loaded in porous PLGA scaffolds (**C**, scale bar, 100 μm). **(D)** Microencapsulated IGF1 was sustainably released in the tested 4 wks. Adipose tissue formation within a representative PLGA scaffold with IGF1 microspheres following 4-wk implantation in the inguinal fat of C57Bl6 mice showing overall dimensions maintained (5×3 mm) **(E)** (scale bar, 1 mm). A representative IGF1-free PLGA scaffold following 4-wk *in vivo* implantation showing modest tissue ingrowth **(F, G)**. A representative IGF1 delivered scaffold showed adipogenesis and adipose stroma **(J, K)** (**F, J**, scale bar, 200 μm; **G, K**, scale bar, 50 μm). Adipocyte number was counted based on morphology in the slides and the relative area was determined by the percentage to scaffold area. The number of adipocytes and adipocyte area were significantly greater in IGF1 delivery scaffolds than IGF1-free scaffolds **(N, O)** (mean ± s.d., n=3, ***p<0.001, ANOVA). No FABP4 expression in IGF1-free scaffolds (**H**), and FABP4 staining in IGF1 delivery scaffolds confirmed adipose tissue formation (**L**) (scale bar, 50 μm). Anti-CD146 antibody staining showed the absence of CD146+ cells in IGF1-free scaffold **(I)** and the presence of CD146− and CD146+ cells in IGF1 delivered scaffold **(M)** (scale bar, 50 μm).

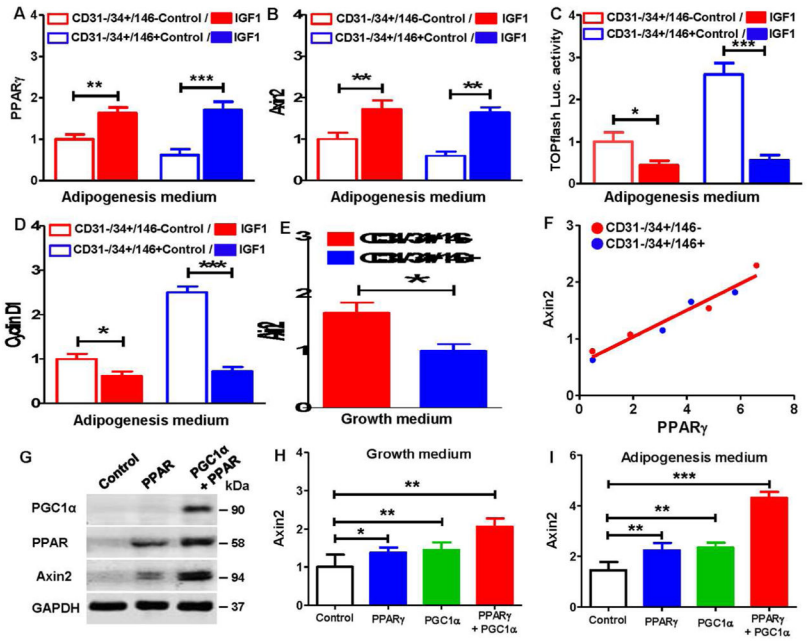

Figure 6. Axin2/PPARγ signaling activates adipogenesis

PPARγ **(A)** and Axin2 **(B)** showed significantly higher expression in CD31-/34+ cells upon IGF1 induction, regardless of CD146 polarity, but significantly attenuated TOPflash luciferase activity **(C)** and cyclin D1 mRNA expression **(D)**. Native CD31-/34+/146− cells showed significantly higher Axin2 level than CD31-/34+/146+ cells **(E)** (mean ± s.d., n=3, *p<0.05, **p<0.01, ***p<0.001, Student's t-test). Axin2 and PPARγ showed positive correlation in CD31-/34+ cells, regardless of CD146 polarity **(F)**. PPARγ and/or PGC1α induced Axin2 expression by Western blot, GAPDH served as an internal control **(G)**. Stromal vascular fraction cells over-expressed with PPARγ and/or PGC1α showed significantly higher Axin2 expression in growth medium **(H)** and adipogenesis medium **(I)**. Knockdown of PPARγ and/or PGC1α **(J, K, L)** with corresponding siRNAs significantly attenuated Axin2 expression in SVF cells **(M)** (mean ± s.d., n=3, *p<0.05, **p<0.01, ***p<0.001, Student's t-test).

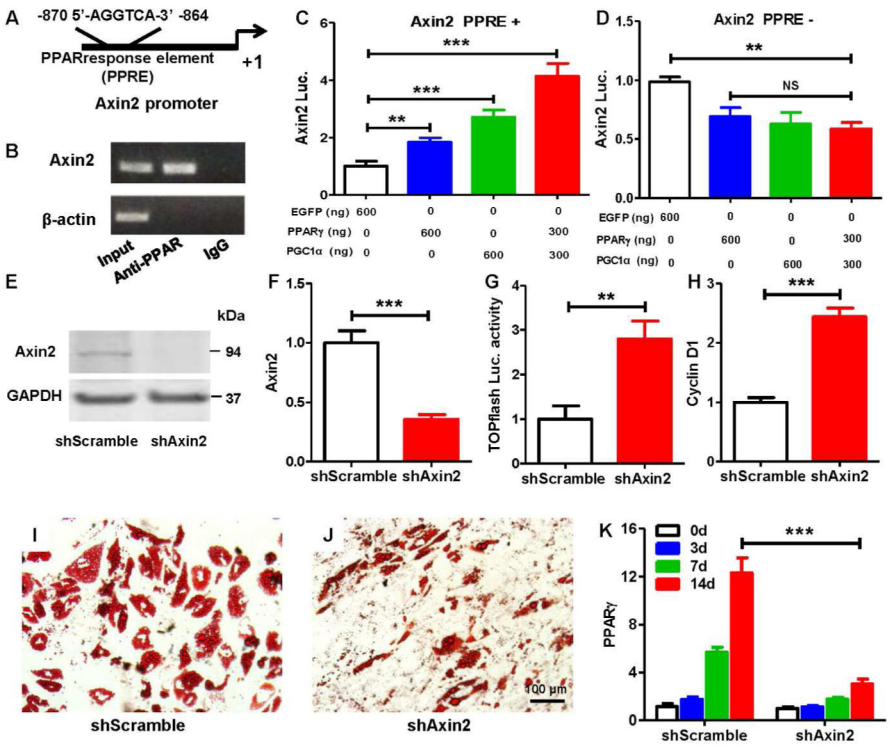

Figure 7. PPARγ transcriptionally activates Axin2 in adipogenesis

Schematics of Axin2 promoter with ~1000 bp upstream of Axin2 translation start site (ATG) with a putative PPRE **(A)**. ChIP analysis revealed binding of PPARγ to Axin2 PRE promoter region **(B)**. Stromal vascular fraction cells (SVF) exposed to adipogenic differentiation medium for 4 days and then harvested for luciferase report analysis, showing that Axin2 PPRE induced Axin2 luciferase activity in the presence of PPARγ and/or PGC1α **(C)**. Without Axin2 PPRE, Axin2 luciferase activity was attenuated even in the presence of PPARγ and/or PGC1α **(D)**. Axin2 knockdown with shAxin2 transfection showed Axin2 absence **(E)** and severely attenuated **(F)**, with shScramble served as negative control. TOPflash luciferase activity and CyclinD1 were upregulated following Axin2 knockdown **(G, H)**. SVF cells showed adipogenesis **(I)** that is remarkably reduced following Axin2 knockdown **(J)** (scale bar, 100 μm). PPARγ increased in SVF cells undergoing adipogenesis but was attenuated by Axin2 scrambling in the tested 14 days **(K)** (mean ± s.d., n=3, *p<0.05, **p<0.01, ***p<0.001, ANOVA).